Seasonal mobility of transverse finger bars within a mixed sand-gravel bay measured using X-band Radar

Dominique Townsend [a,*], Julian Leyland [a], Hachem Kassem [b], Charlie E.L. Thompson [b,c], Ian H. Townend [b], Paul S. Bell [d], Cai O. Bird [e]

[a] School of Geography and Environmental Science, University Road, Southampton, Hampshire SO17 1BJ, UK
[b] School of Ocean and Earth Science, University of Southampton, Waterfront Campus, National Oceanography Centre, European Way, Southampton SO14 3ZH, UK
[c] Channel Coastal Observatory, Waterfront Campus, National Oceanography Centre, European Way, Southampton SO14 3ZH, UK
[d] National Oceanography Centre, Joseph Proudman Building, 6 Brownlow Street, Liverpool L3 5DA, UK
[e] CoastSense Ltd, 320 Mariners House, Liverpool L1 0BG, UK

ARTICLE INFO

ABSTRACT

Transverse finger bars have largely been associated with sandy coasts. Here we show that these features persist within a wider mixed sediment environment, adjacent to a shingle cuspate foreland, which has not been previously reported. Details of the bars' characteristics were gleaned from analysis of bathymetry data, whilst weekly migration rates were inferred from remote sensing of the sea surface roughness as a proxy of undulating bedforms, using X-band radar reflectance data. The bars were on average ~380 m long, had wavelengths of ~160 m, amplitudes of approximately 0.2 to 0.6 m and were orientated 30° to shore normal. They were found in water depths between −3.3 and −5.8 m Ordnance Datum. The bars migrated by approximately 150 m over the first 'winter' observation period (15/11/2020–02/04/2021) and 70 m in the following winter period (Sept 2021–Feb 2022) but showed virtually no signs of movement during the intervening summer months. Analysis of hydrodynamic conditions suggested the bar mobility was related to the dominant longshore currents resulting from high angle, south westerly waves. Low amplitude rhythmic bedforms were also found in the upper beach, migrating at a similar rate to the nearshore bars, which are thought to be driven by high-angle wave instability.

1. Introduction

Shallow seas, extending to 200 m depth, occupy around 7.5 % of the ocean. Across the world, this area is made up of an incredibly diverse range of sediments, geological and geomorphological features. Amongst the most striking of these features are rhythmic bedforms, with wavelengths ranging in scale from centimetres to 100s of metres, they are found in both deep and shallow water (Amos and King, 1984; Boczar-Karakiewicz and Bona, 1986; Swift et al., 1978). Of these, ripples, dunes, and bars are known to form as near bed flow exceeds a critical velocity, which is dependent on grain size. In the right conditions, these features migrate, usually in the dominant direction of flow, transporting sediment in the process. Whilst the conditions for small scale bedform formation can be easily recreated in the lab, there is less confidence in the formation of larger scale features, especially those found within the nearshore zone, *i.e.* the zone affected by waves and tides, where behaviour is complex and subject to a number of non-linear interactions

between waves, currents and the underlying topography itself (Chen et al., 1999; Holman, 1995; Touboul et al., 2024). Observational data from the nearshore zone is typically scarce and hard to come by as it is both expensive and can be challenging to collect. This study uses a unique high temporal resolution dataset collected using X-band radar to study the movement of a series of transverse finger bars in an environment in which they have not previously been observed, and links their mobility to driving forces and theory.

Transverse bars, *i.e.* bar like features which lie approximately normal to the shoreline orientation (Shepard, 1952), are reported globally, in various forms on open coast, tidal inlets and sheltered backwaters (Falqués et al., 2021; Konicki and Holman, 2000; Pellón et al., 2014; Ribas and Kroon, 2007). Their cross-shore extent has been found to range in scale from 10s to 1000s of m (Carter, 1978; Gelfenbaum and Brooks, 2003); they have been found in both microtidal and macrotidal coasts (Konicki and Holman, 2000; Levoy et al., 2013); and there is no universal agreed formation mechanism (Falqués et al., 2021). Niedoroda
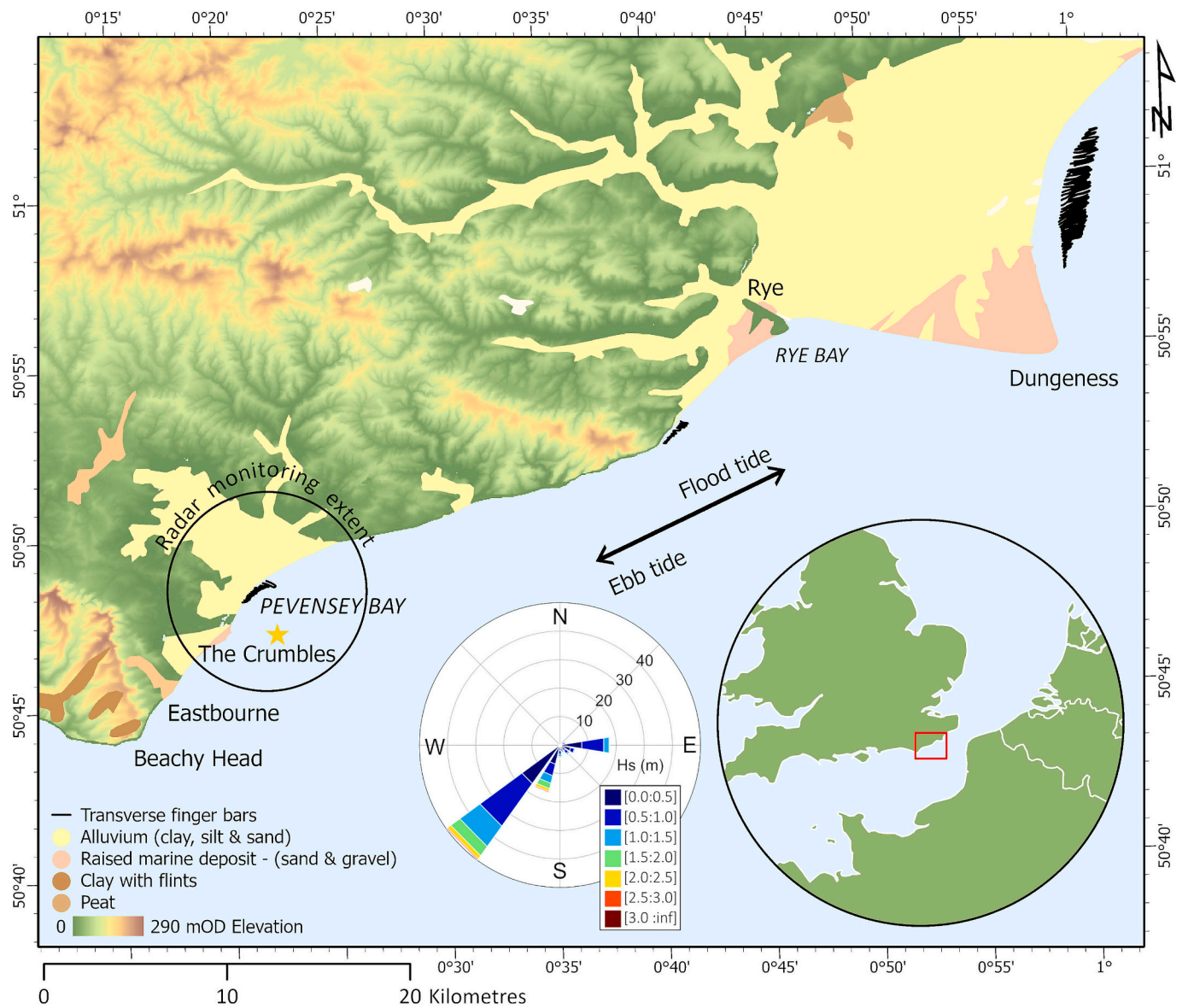
Fig. 1. Transverse finger bar locations in relation to the Crumbles and Dungeness cuspate foreland formations with regional setting inset. Star shows location of the Datawell MkIII directional wave buoy within Pevensey Bay, which is part of the NNRCMP network (channelcoast.org). The data from this wave buoy between June 2003 and November 2022 is shown binned as a wave rose. Figure contains Ordnance Survey Terrain 50 open height dataset © Crown copyright and database right 2023.

and Tanner (1970) described the bars as equilibrium features, forming (permanently or ephemerally) when sediment transport, waves and currents were balanced. Pellón et al. (2014) grouped transverse bars into four groups: transverse bars and rips, large-scale finger bars, finger bars of intermediate beaches and low energy finger bars. Note that the term 'finger' is used to describe bars where the cross-shore length of the bars exceeds the alongshore width, giving a finger like appearance (Niedoroda and Tanner, 1970). 'Transverse bars and rips' are not discussed further here as their formation is due to the onshore welding of crescentic bars, enhanced with rip flow which is different from the other types of transverse bar explored below, and unlike those found within the study site. Instead, we focus on finger bars, collectively comprising three of Pellón et al.'s (2014) transverse bar groups:

- **Large-scale finger bars** are distinguished from other finger bars by their magnitude, with cross-shore extents typically exceeding 1000 m (Pellón et al., 2014). They are found on very shallow, low wave energy coasts, and observations of annual migration rates are low,

not exceeding 10–20 m per year (Gelfenbaum and Brooks, 2003; Goud and Aubrey, 1985; Niedoroda and Tanner, 1970). These features have been observed over long time periods (in excess of 40 years) and are also typically orientated normal to the shoreline. Additionally, large scale finger bars have been reported on macro-tidal coasts, in the vicinity of ebb tidal deltas and inlet systems (Brakenhoff et al., 2019; Levoy et al., 2013).

- **Intermediate energy finger bars** are ephemeral features which can form under certain constant wave conditions, consisting of oblique intermediate energy waves (Ribas et al., 2003). They are of a smaller magnitude than the large-scale finger bars, (~100s m), can be associated with nearshore bars, and are up-drift orientated (Konicki and Holman, 2000; Ribas and Kroon, 2007).

- **Small scale finger bars** are found in fetch-limited areas (<10 km), and are persistent, downdrift orientated features. They have been shown to migrate during stormy periods, with limited movement during summer periods, although measurements of migration rates are limited (Pellón et al., 2014).
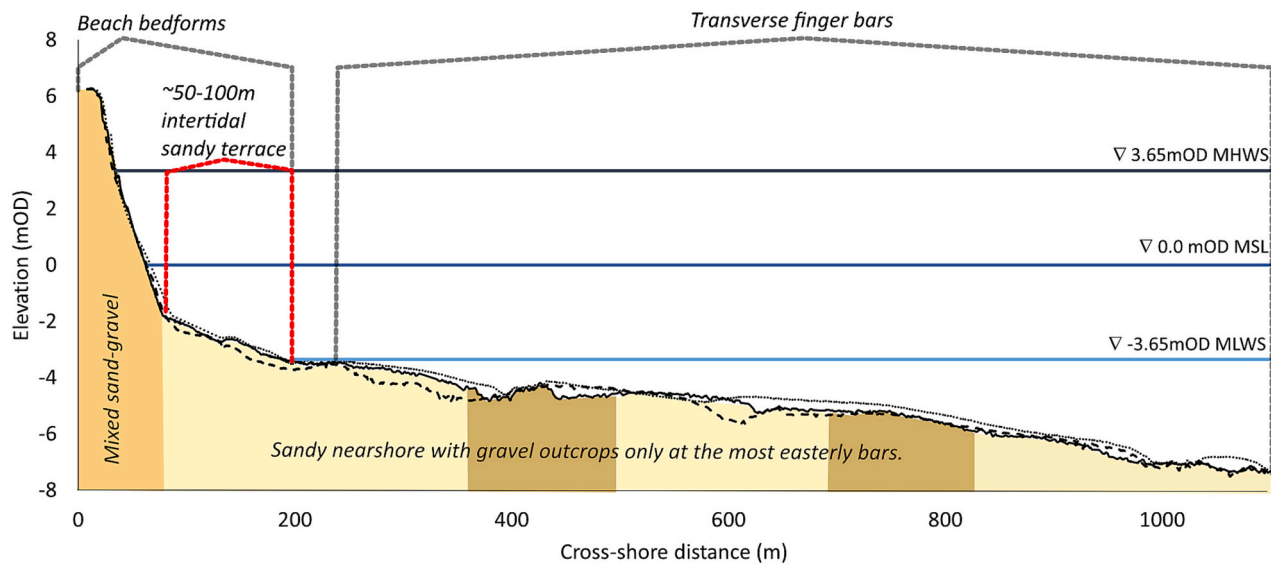
Fig. 2. Cross section of typical profile within the barred section, showing tidal range and beach profile. Adapted from Townsend et al., 2024.

There are two key theories on the formation of transverse finger bars: the forcing template theory and the self-organisation theory. The first theory, forcing template theory assumes a fixed flow, caused by low-frequency standing edge waves, or progressive infragravity waves, which can moderate shoreline morphology (Guza and Inman, 1975). Edge waves are formed by infragravity waves becoming 'trapped' at the shoreline, due to refraction and reflection effects. Studying the Atlantic shelf of North America Boczar-Karakiewicz and Bona (1986) reasoned that linear sandy ridge bedforms with wavelengths in the order of km, must have been formed by infra-gravity waves with periods between 0.5 and 5 min as only they would be large enough to drive the formation of these bedforms. However, forcing template theory has since been questioned in the context of transverse bars, as it ignores any feedback of the bedforms onto the hydrodynamics (Coco and Murray, 2007; Ribas et al., 2015). Furthermore, infragravity waves are known to be progressive and move much faster than the bedform migration (Ribas et al., 2015). The second theory of self-organisation was initially suggested by Sonu (1968) suggesting that the formation of transverse bars is caused through positive feedbacks, between longshore hydrodynamic processes (longshore currents) interacting with uneven bathymetry. Falqués et al. (2021) also recognized the potential for cross-shore processes to create positive feedback between wave refraction and bars for shore-normal wave incidence in case of very shallow terraces, *i.e.* sandy deltas. On the basis of self-organisation theory, several linear and non-linear stability analyses have successfully predicted the number, spacing and amplitude of bars on straight coasts, although they have been found to overestimate migration rates (Falqués et al., 2008; Ribas et al., 2011; Ribas and Kroon, 2007). Further developments show that cross-shore variations in the depth-averaged sediment concentration play a highly important role in determining whether bar features are orientated up or down-drift relative to the predominant current (Ribas et al., 2015).

Although some progress has been made in studying these bars in the last 30 years, the available measurements of their characteristics, migration rate and sedimentological properties are sparse (Pellón et al., 2014; Ribas et al., 2015). Studies thus far have almost solely explored features found on sandy, microtidal and straight coastlines (Brakenhoff et al., 2019; Levoy et al., 2013; Schupp et al., 2006). This study aims to expand the current knowledge of these systems by reporting these bar characteristics for the first time on the lee side of a cuspate foreland within a macro-tidal, mixed sediment environment. A thorough investigation of the bars' morphology and behaviour was undertaken through the quantification of bar characteristics, surficial sedimentology, seasonal migration rates and efforts to understand the wider geomorphological setting of the study site.

1.1. Study site

The study site, Pevensey Bay, is a composite, mixed sand and gravel barrier beach located on the South East coast of the UK. The barrier beach fronts approximately 50 km^2 of freshwater low-lying alluvial deposits which were reclaimed from the sea in the 14th century for farming purposes (Hartmann, 2017). The low lying land is bordered to the west by the chalk ridge and headland the South Downs, terminating at Beachy Head, and the Wealden uplift formation to the east (Fig. 1, Sutherland and Thomas, 2011; Jennings and Smyth, 1990). The beach is largely fronted by a gently sloping sea bed (slope grade 0.0064–0.0069) which steepens at the western extent (slope grade 0.16.) and is partially constrained in the nearshore by rock outcrops at the western extent of the site (Fig. 1; Townsend et al., 2024). Subtidal bed sediments are complex mixtures of sands and gravels with some mud occasionally detected (Townsend et al., 2024), with evidence for drowned barrier beaches further offshore (Mellett et al., 2012). There is no evidence for present day onshore migration of these large gravel deposits (Nicholls, 1991). The gravel barrier which makes up approximately three quarters of the length of the site conjoins with a cuspate foreland, known locally as the 'Crumbles' (Fig. 1). Pevensey Bay is a local depocentre, *i.e.* the area of greatest sedimentation over the medium- to long-term (Halcrow, 2010), and gravel deposits at the site have been reported to be approximately 33 m deep (Jennings and Smyth, 1990). The cuspate foreland was formed between 800 and 300 years before present following the vast supply of gravel rich sediment from the west (Nicholls, 1991), and has since been in decline for 300 years (Jennings and Smyth, 1990). In 1993 the Crumbles cuspate foreland was excavated and transformed into a large commercial harbour, with two rubble mound breakwaters constructed at the entrance (Sutherland and Thomas, 2011). This interrupted the natural flow of sediment and to counter this loss, approximately 110,000 m^3 of sediment is recycled, renourished and bypassed into the Pevensey Bay frontage each year, to maintain the volume of the beach which serves as an important flood defence. Approximately 40 km down drift (east) of the Crumbles site, is the much older and larger cuspate foreland system of Dungeness (Plater et al., 2009, Fig. 1). Transverse finger bar formations are visibly present to the east of both cuspate forelands.

Pevensey bay is predominantly exposed to south westerly waves (Hs ≤2.5 m) close to 85 % of the time and less frequently, smaller easterly waves (Hs ≤1.5 m) around 15 % of the time (Fig. 1, Sutherland and

Thomas, 2011). In a typical year, wave conditions are calmest between April and August (Hs ~0.6 m), and more energetic between September and March, with average monthly Hs peaking at just over 1.0 m in December (National Network of Regional Coastal Monitoring Programmes., n.d.). The spring/neap tidal range is 6.7 m and 2.3 m respectively, with a lowest astronomical tide limit of −3.65mOD and depth of closure varying between −7.3 to −8.2mOD across the bay over a decadal timescale (Elsner et al., 2015; Horn and Walton, 2007; Townsend et al., 2024). Depth averaged tidal currents vary throughout the tidal cycle with an average rate of 0.3 ms^{-1} during mean neap tide conditions and up to 0.5 ms^{-1} during mean spring tide conditions (Fugro Emu, 2016). The currents are rectilinear and usually flood dominant. The non-tidal current component has been shown to flow up to 0.71 ms^{-1}, although average flows are typically between 0.04 and 0.11 ms^{-1}.

This study examines the transverse finger bar features found in the shallow nearshore (subtidal) and the rhythmic bedforms located in the intertidal upper beach as shown in Fig. 2. The steep reflective upper beach is comprised of mixed sandy gravel, with a median grain size (D_{50}) ranging between 8 and 12 mm across samples (Dornbusch et al., 2005), and the shallow sandy terrace fronting the upper beach is formed of fine sand with a median grain diameter of fine sand, 159–164 μm (Townsend et al., 2024).

2. Methods

2.1. Bar characteristics measured using MBES

The physical characteristics of the transverse finger bars at Pevensey Bay were measured from Multi Beam Echo-Sounding (MBES) data, recorded on the 01/08/2013. The MBES bathymetry survey was commissioned by the National Network of Regional Coastal Monitoring Programmes (NNRCMP) for England and carried out by EGS International Ltd. The survey extended from Mean Low Water to approximately 1 km offshore with 100 % seafloor coverage to International Hydrographic Office (IHO) Order 1a standard, and meeting the Maritime & Coastguard Agency (MCA) Civil Hydrography Programme Survey Specification 2013 (Channel Coastal Observatory, 2014). A Kongsberg EM3002D MBES was used to capture the data, which were processed in IVS Fledermaus version 7.3, by QPS Ltd. Quality-control of the data was undertaken by the United Kingdom Hydrographic Office (UKHO). The data analysed here were downloaded from the Channel Coastal Observatory website (channelcoast.org) and comprised 1 m resolution data, projected to OSGB/Ordnance Datum (OD). For each bar: the length, wavelength (*i.e.* crest to crest distance), the most landward and seaward depth along the bar crest, form (chevron/linear) and angle (both to °TN and relative to shore normal, whereby the shore normal is a right angle to the low-tide contour) were recorded. Contours were generated at every 0.1 m relative to Mean Sea Level (MSL) which were used as a guide to measure the features within GIS software, ESRI's ArcGIS Pro version 3.0.2. The crestlines of the features were digitized from the point at which the first contour deformation was identified, to the deepest deformed contour, marking the base of the feature. In some instances the orientation of the bar crestline changed direction, forming what we term a 'chevron' morphology. For these features a vertex was recorded at the junction of the change in crestline, and measurements were given for both the 'upper' and 'lower' section of the bar, as well as the combined measurements. The landward and seaward depths were measured from the start and end of these digitized lines, respectively, and the angle was calculated from the landward 'start' and seaward 'end' of each bar, relative to both true north and shore normal. Elevations relative to mOD were extracted every meter along a shore parallel transect, approximately 350 m offshore, which coincided with the mid-point of the crest for the majority of the transverse finger bars. Stoss and lee slopes were calculated for each bar included within the transect from the highest and lowest points respectively.

2.2. Sedimentology

Fifteen van Veen grab samples were retrieved along a shore-parallel transect within the transverse finger bar area on the 25/09/2022. The transect was approximately 250 m from the shore and the samples were taken between 10 and 50 m apart, spanning a length of ~800 m. Grain size analysis was completed complying to BS EN ISO 17892-4:2016. Samples were washed to remove salts over a 63 μm sieve, retaining the water and visually checking the water colour for any indication of fine sediments, none were found. The samples were then dried in an oven and sieved with an Octagon200 sieve shaker, with ¼ phi mesh size grading, before weighing. Median grain size, sorting, skewness and kurtosis were calculated using the arithmetic method of Krumbein and Pettijohn (1938) using the Gradistat software (Blott and Pye, 2001).

2.3. Bar movement

X-band Radar reflectance imagery was used to detect the presence and migration of bedform features; Section 2.3.1 describes the theory behind the method, and Section 2.3.2 outlines the workflow used in this paper. The raw processing of the radar data and sea surface roughness images were carried out by Marlan Maritime Technologies Ltd. (now CoastSense Ltd).

2.3.1. X-band radar & sea surface roughness

Radar (Radio Detection And Ranging), is the concept of accurately identifying a target and measuring its distance from the radio antenna signal's origin point (*i.e.* a Radar transmitter), using the basic relationship between speed and time. X-band Radar waves have a wavelength of 2.5 cm to 3.8 cm, with a frequency ranging between 8 and 12 GHz, which allows them to measure gravity waves on the sea surface in the presence of Bragg scattering (Nieto-Borge et al., 2006). Bragg scattering is caused by the presence of capillary waves (mm scale wavelengths) superimposed on gravity waves (cm to m scale), which creates a texturally rough sea surface. This sea surface can be modulated further when fast flowing tidal currents flow over uneven bedform topography resulting in divergent flow, as turbulent vortices (kolks) are generated in the lee of the bedforms and 'boil' to the surface (Alpers and Hennings, 1984). Following this 'rougher' patch of water, convergent flow 'smooths' the sea surface. Whilst it is not possible to identify these 'smooth' and 'rough' patches of sea from individual snapshots in time, composite Radar images can provide information on surface roughness (Bell et al., 2015).

2.3.2. Sea surface roughness to detect bedforms

A GEM Elettronica SuperNET with a 2.2 m radar antenna and a 12 kW peak output power mounted was fitted to a lighting column mounting (Bird et al., 2019) and deployed at Pevensey Bay (50°48′51.5″N 0°21′30.3″E) between 11/11/2020 and 28/02/2023, with the antenna located at approximately 17 mOD, during which time it operated continuously until 25/09/2021. After this period, to avoid disturbing local residents the Radar operated on an event-based protocol, when wave conditions were forecast to exceed 1.5 m at the nearest wave buoy (50°46′54.6″N 0°25′06.0″E). During operation, Radar reflectance images were captured every 0.86 s covering a radial area of 6 km (4096 by 4096 pixels, 50° 52′ 4.062″N 0° 16′ 7.9176″E to 50° 45′ 38.6712″N 0° 26′ 54.0024″E), and approximately 12 km of coastline (2 km of which were shadowed by the cuspate foreland).

Raw (analogue) radar data were translated to digital signals in real-time by a 50 MHz digitiser and computer located within the column of the Radar tower, where they were also stored. Most analogue ship radars have an intermediate frequency (IF) bandwidth cutoff at around 18 MHz, limiting the amount of 'information' that can be carried by the signal, so the output video signals that are digitized are inherently limited in horizontal resolution to around 10 m–20 m. The 50 MHz digitisation rate is tailored to capture the maximum possible
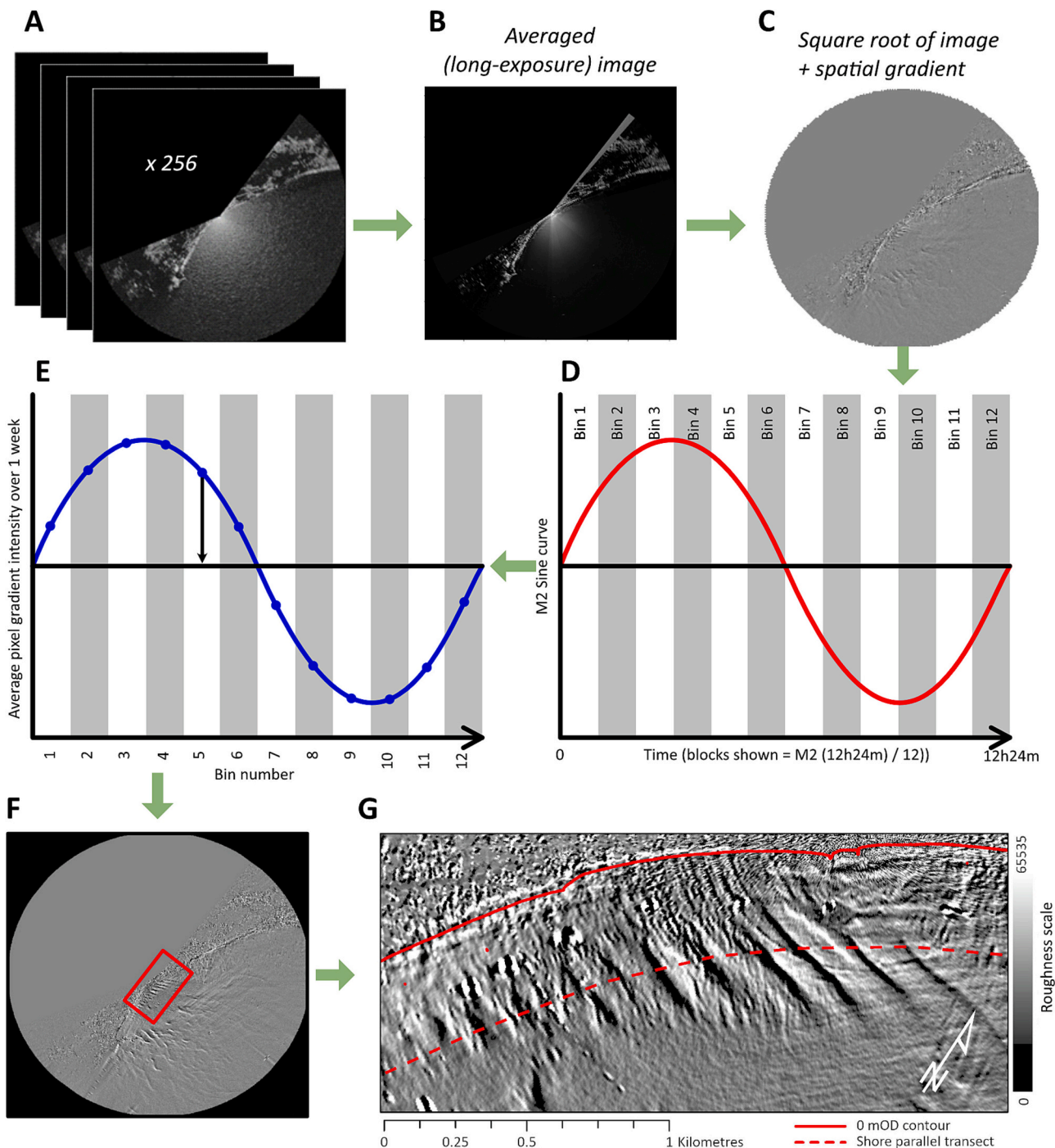
Fig. 3. A) 256 raw radar images (representing about 5 min real time); B) long exposure image (an average of the 256 images); C) image where each pixel has had the square root then spatial derivative taken; D) images are binned into 12 M2 tidal phase bins; E) the tidal signal is removed by fitting an M2 sine wave to average pixel values per bin (per week) and then subtracting that value; F) the resultant sea surface roughness image with extent of; G) Zoom-in of F with 0mOD and shore parallel transect overlain.

information from such signals.

Once retrieved, the raw data were transformed from polar to cartesian co-ordinates with a x resolution of 4.38 m and a y resolution of 2.61 m to the WGS 1984 geographic co-ordinate system (Fig. 3, A). A near real-time telemetry system then transferred these data to a server housed in the Marlan office in Liverpool, UK, where the sea surface roughness analysis was carried out.

The principle of the radar roughness analysis is to detect subtle, tidally modulated sea surface roughness variations that can be an indication of the interaction of tides, waves and currents with relatively

small-scale subsurface sea bed features. Such roughness features may not be detectable in individual radar records, but a time series analysis over a number of tides can average out more ephemeral phenomena, revealing the sea surface signatures of more persistent features.

Whilst the analysis could be run on a single tide of data records in optimal conditions where sufficient sea surface signatures are present, 1–2 weeks of data are more optimal to reduce the noise and variability introduced from individual weather events and overcome periods of calm seas from which radar backscatter can be insufficient for detection of any sea surface signatures at all. Features of the scale of the finger bars

discussed here are unlikely to migrate significantly within such a short time window, although smaller, more ephemeral sea bed sediment features may come and go at that timescale.

The analysis procedure follows the flow diagram of Fig. 3. Data bursts of 256 images were averaged to a single long-exposure image to remove wave signatures and other ephemeral signals representing 15 min in time (Fig. 3, A–B). The gradient of the long-exposure image is then calculated to highlight small scale structures in the signals (Fig. 3, C). These gradient images were then binned into one of 12 tidal phase bins, associated with the M2 tidal period divided by 12 (Fig. 3, D), which allows backscatter/roughness sources from both currents (which peak at mid tide) and waves (which peak at low tide) to be included within the final image. After a week of data have been phase-binned in this way, an M2 tidal signal is fitted to each pixel (Fig. 3, E). The fitted M2 signal provides an indication of subsurface sea bed features that influence sea surface roughness at a local scale (Bell et al., 2015). The weekly periods began at 00:00 Monday morning and finished at 23:59 Sunday evening, producing 47 sea surface roughness images over the total period of operation (Fig. 3, F). In some instances, especially during the intermittent operation period, the number of images recorded was less than during normal operation; for instance, if the Radar were switched on from Monday to Wednesday, of one week, significantly fewer images would be included within that sea surface roughness image. This is not thought to impact the overall results as the strongest signals are captured during the wave events, whilst during calmer conditions, all of the radar backscatter values are lower and contribute less to the overall imaging of the features.

The files were stored in Geo tiff file format with an arbitrary measurement unit, ranging between 0 and ~65,000 (Fig. 3, F–G). The sea surface roughness gradient images were then imported into GIS Software, and the values were extracted every meter along the shore parallel transect (Fig. 3) which was previously utilized in the MBES analysis, with an aim to capture the mid-point of the crest for the majority of the transverse finger bars.

2.4. Hydrodynamic analysis

To understand the drivers behind bar mobility (between November 2020 and Feb 2022), wave records were analysed from the Datawell MkIII directional wave buoy, located within Pevensey Bay in approximately −9.8 m water depth (50° 46.91′ N 0° 25.10′ E, shown as star in Fig. 1). The wave buoy is part of the NNRCMP network of wave buoys; the data are freely available to download from https://coastalmonitoring.org/. First, daily, and monthly mean values were calculated for the peak wave direction and wave power, which were calculated by the NNRCMP as part of a QC process, for comparison to the Radar observation period.

Secondly, littoral drift potential was estimated for the area of transverse finger bars. This was done using Soulsby's simplified version of the CERC transport equation (Soulsby, 1997):

$$Q = \frac{0.023g^{\frac{1}{2}}H_{sb}^{\frac{5}{2}}sin(2\alpha_b)}{(s-1)} \tag{1}$$

where g is acceleration due to gravity, H_{sb} is the significant wave height at the breaker line which is dynamically assessed based on Weggel's (1972) work relating bed slope to breaking wave height, α_b is the angle between wave crest of the breaking wave and the shoreline, and s is the relative density of the sediment. The significant wave height and wave crest angle was attained by transforming the wave record from the Pevensey Bay wave buoy (Fig. 1) to a nearshore point at the edge of the surf zone using linear wave theory. Water depths were estimated with records from the Newhaven tide gauge, which lies approximately 20 km west of Pevensey Bay (50° 46.907′N, 0° 3.422′E). The transformation of the nearshore waves and littoral drift potential were calculated in CoastalTools, a freely available MatLab App (https://github.com/C

Table 1
Data collected as part of the National Network of Coastal Monitoring Programmes of England NNRCMP used in the analysis of upper beach volumetric analysis.

Available DTMs	Survey type	DTM Resolution	Difference models	Analysis carried out by
2003–2005 2007 2009–2011	GPS walked/ quad survey	1 m	2003–2004 2004–2005 2005–2007 2007–2009 2009–2010 2010–2011	Canterbury City Council (on behalf of Environment Agency)
2012–2015	Terrestrial laser scan	1 m	2011–2012 2012–2013 2013–2014 2014–2015	
2015–2022		Various: 0.5, 1 & 2 m	2015–2016 2016–2017 2017–2018 2018–2019 2019–2020 2020–2021 2021–2022	University of Southampton

oastalSEA). A detailed description of the nearshore wave transformation is available in the supplementary material of Townsend et al. (2024).

2.5. Upper beach volumetric analysis

A geospatial analysis calculating volumetric change between topographic surveys over time for the length of the study area within 50 m bins has been performed over a 19-year period. The analysis used topographic data collected by Adur &Worthing Councils, as part of the NNRCMP (Table 1). The topographic surveys covered the entire upper beach, from the backshore to seawards of the beach toe, *i.e.* the point at which the steep mixed sand-gravel upper slope transitions to a flatter, sandier slope, down to the low water mark at the time of the survey. Before 2012, surveys involved backpack/quadbike mounted RTK GPS surveys, whilst from 2012 onwards, the survey is conducted using a quadbike mounted laser scanner. After quality checking the data, Triangular Irregular Network (TIN) surfaces are generated from individual points, and then converted into Digital Terrain Models (Table 1). Additionally, the laser scan data undergo a filtering process, removing any points above a set height which is determined per survey site, clipping the data (based on survey extents which helps exclude seawalls for example) and a further bare-earth classification, which ensures only the ground points are used to create the DTM (Dan Amos, *pers. comm*). This removes any unwanted points, *e.g.* sunspots, people, birds *etc.* The data are freely available to download from the NNRCMP website; www.channelcoast.org.

Difference models, *i.e.* a surface model showing change in elevation between two time periods, were calculated between annual topographic surveys (Table 1), the majority of which were carried out in the winter period (October–April) with an aim to consistently represent the beach at its lowest, following any winter offshore movement of sediment. The difference models were calculated in GIS Software ArcGIS Pro, whereby the 'Raster Calculator' function was used to subtract the older grid data from the newer grid data to give the difference in elevation. The site was dissected by a series of polygon features; 50 m wide in the longshore direction by 500 to 1000 m in cross-shore length. To accommodate changes in the orientation of the coastline, the orientation of the polygons changes from 120°TN to 155°TN at approximately 3000 m chainage, resulting in 4 polygons with a reduced areal extent. To understand the total volume change that occurred within each 50 m polygon, the sum of the pixels from the difference model that fell within each polygon was calculated. The volumetric change within the polygons for each difference model was calculated in ArcGIS using the 'Zonal Statistics as
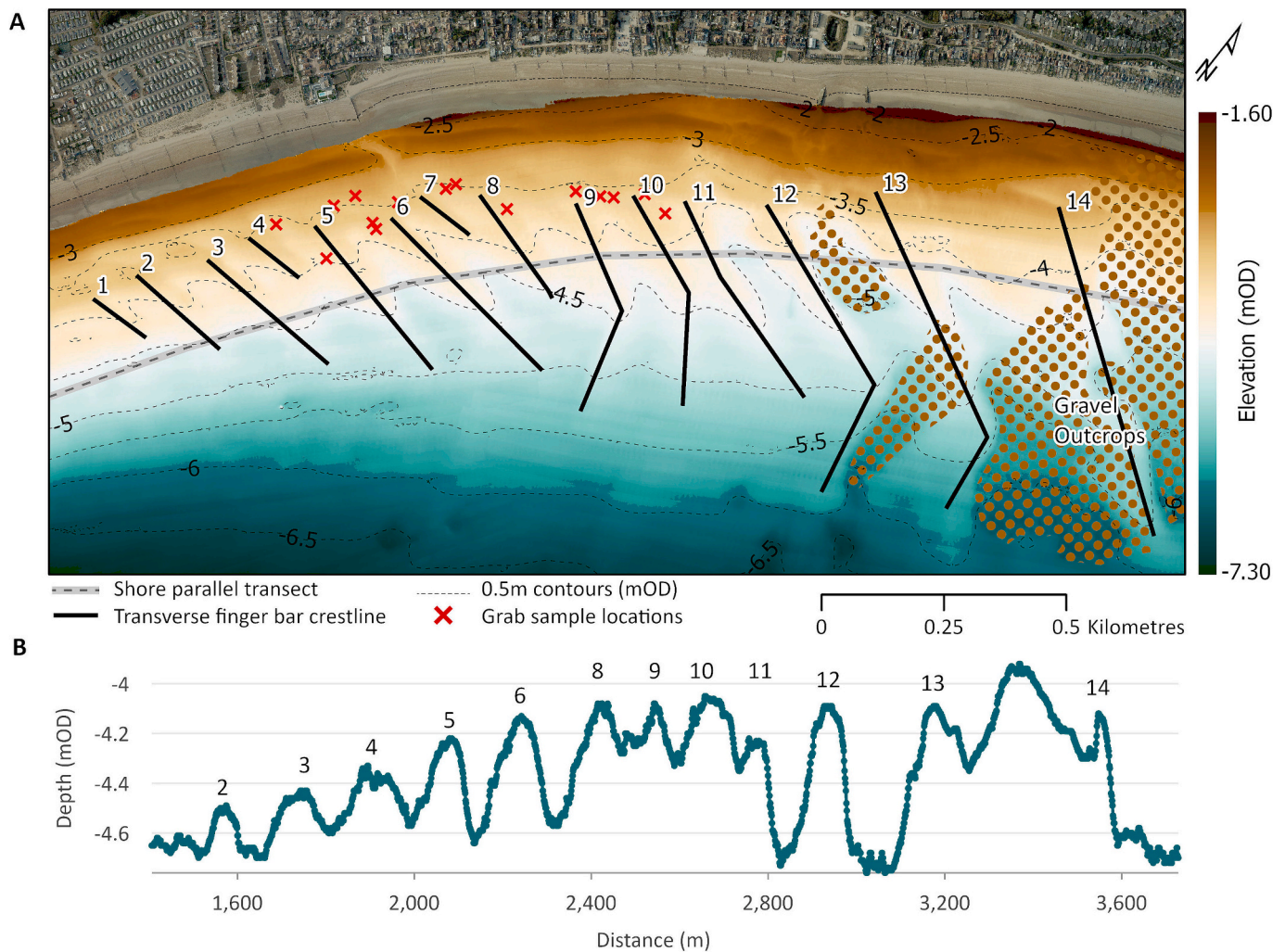
Fig. 4. A) Bathymetry of 14 transverse finger bars showing gravel outcrops to the east, smoothed 1 m contours, with orthorectified aerial photography (both collected as part of the NNRCMP). Note the presence of two surface water outfalls just north of the 13th bar; B) Cross section through the bathymetry data along the shore parallel transect (350 m offshore) showing local elevation of bars. N.B. the first bar does not extend out to the shore parallel transect and is therefore intentionally not labelled in panel B.

Table' tool, whereby the elevation difference (m) per unit area (m²) is summed to produce a total volume. If the resolution of the pixels were greater or <1 m, the result of the sum was adjusted accordingly (Table 1). For example, a 2 m resolution raster would be multiplied by four, whilst a 0.5 m resolution grid would be divided by four, to convert the elevation change over 0.5/2 m squared to 1 m squared respectively which could then properly reflect the volume change (m³). This work was an extension of analysis performed by Canterbury City Council on behalf of the Environment Agency as part of a Regional Shingle Beach Management Plan, which originally only covered the time period from 2003 to 2015 (Environment Agency, 2017). The transect area GIS shapefile is available as supplementary information.

3. Results

3.1. Bar characteristics

Fourteen transverse finger bars were observed in the MBES bathymetry data from 2013 (Fig. 4). The bars ran parallel to each other, adjusting to changes in shoreline orientation. A cross section (approximately 350 m offshore) through the bars showed a slightly shallower slope on the western flank of the bars, and a steeper slope on the eastern flank (on average 1 in 88 stoss to a 1 in 63 lee slope with a standard deviation of 33 and 15 respectively), indicating eastward migration of the bars (Fig. 4, B; Table 2). Amplitudes of the bars were shown to vary, and at the location of the cross section had local heights varying from 0.2 to 0.6 m (Fig. 4, B). Four of the bars had, what we term, a 'chevron' form, whereby closer to the coast the bars ran parallel with surrounding bars (downdrift aligned) but at some distance offshore had a change in crest orientation, or 'dog-leg' where the lower part of the bars became updrift aligned.

The bars' lengths ranged between 128 and 700 m long (381 m on average, with a standard deviation of 184 m), typically increasing from west to east (Table 2). The distance between one crest to the next (*i.e.*, wavelengths) ranged from 74 and 375 m, with an average value of 156 m (Fig. 4, Table 2). The orientation of the bars (the upper section of the chevron bars) was on average of ~93 °TN for bars 1–8 progressing to ~114 °TN on average for bars 9–14 as the shoreline orientation; the orientation relative to shore normal remained fairly constant at approximately ~30°.

3.2. Sedimentology

Sediment grab samples taken between ~150 and 300 m from the shore spaced at approximately 25 to 100 m from each other (see locations on Fig. 4) showed that the surface sediments were well sorted, all

Table 2

Pevensey Bay bar characteristics measured from 2013 MBES data (Channel Coastal Observatory, 2014). *For those bars with a Chevron form, the length and angles are given for both the upper | lower sections of the bar, with the sum or average given in brackets.

Number	Length* (m)	Distance to next crest (m)	Landward depth (mOD)	Seaward depth (mOD)	Form	Angle (degrees TN)*	angle from shore normal (degrees)*	Stoss:Lee slope (1:X)
1	135	101	−3.5	−4.3	Linear	86	33	–
2	228	148	−3.6	−4.2	Linear	92	30	62:74
3	327	96	−3.6	−4.9	Linear	91	29	104:63
4	132	137	−3.5	−4	Linear	88	35	102:77
5	380	157	−3.5	−4.9	Linear	101	29	93:49
6	439	74	−3.6	−5	Linear	95	26	106:79
7	128	122	−3.5	−3.9	Linear	88	21	–
8	259	197	−3.6	−4.6	Linear	105	28	102:44
9	239 | 222 (425)	118	−3.8	−5.3	Chevron	117 | 163 (139)	24 | −22 (2)	77:44
10	228 | 231 (441)	106	−3.7	−5.2	Chevron	110 | 143 (127)	31 | 0 (49)	70:77
11	472	167	−3.8	−5.1	Linear	109	34	44:48
12	429 | 245 (598)	224	−3.7	−5.7	Chevron	109 | 166 (124)	43 | −27 (23)	118:79
13	551 | 168 (663)	375	−3.3	−5.8	Chevron	116 | 170 (127)	14 | −24 (2)	152:79
14	700	0	−3.3	−5.6	Linear	124	28	26:43
Average	332 | 217 (381)	156	−3.6	−4.9	–	102 | 161 (107)	29 | −18 (19)	88:63
ST. DEV	165 | 29 (184)	82.69	0.15	0.60	–	12 | 10 (17)	7 | 11 (19)	33:15
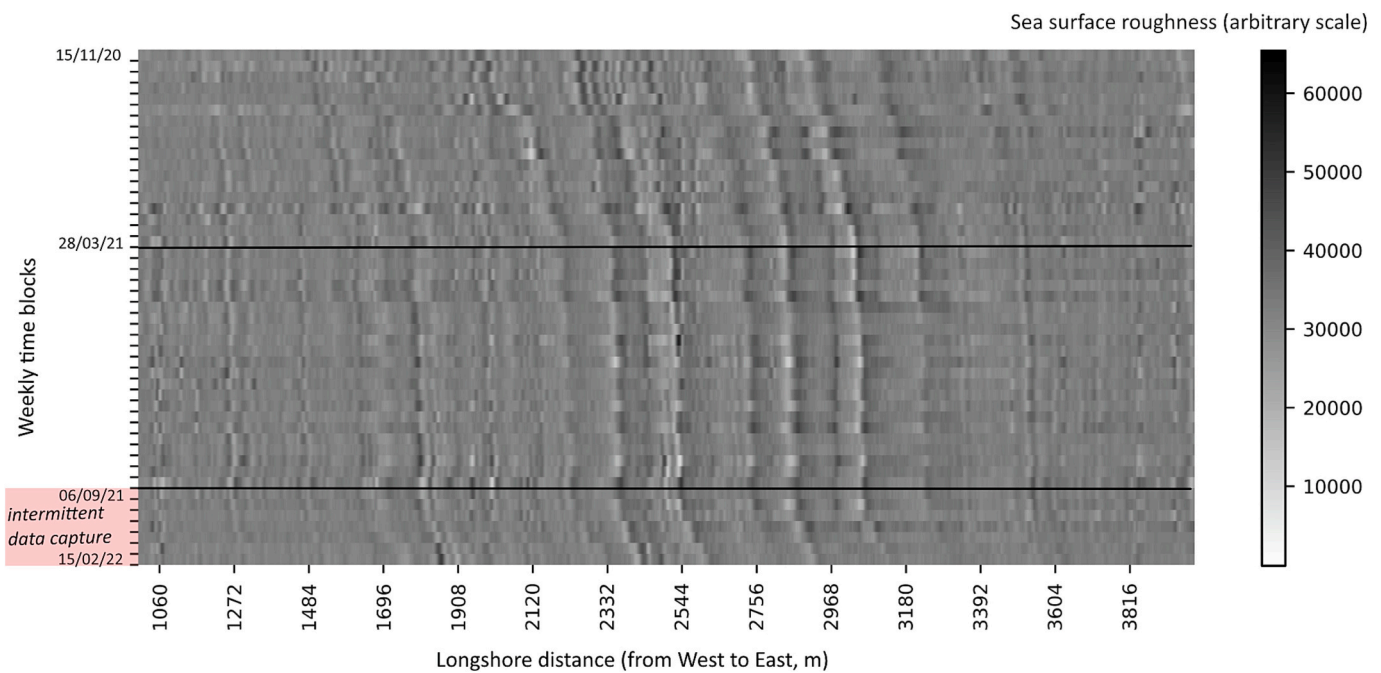
Fig. 5. Sea surface roughness along a transect approximately 350 m parallel to the shoreline indicating the location of the bars and their movement over time. The location of the shore parallel transect is shown in both Figs. 3 and 4.

with a median grain size of 125 μm (very fine sand). The frequency of the samples along the transect was adequate to sample on both stoss and lee sides of the transverse finger bars. No bathymetry data were recorded during the survey, due to equipment failure, so it was not possible to directly relate the positions of the grab samples to morphology of the bars.

3.3. Bar movement

A clear distinction between winter (mobile) and summer (immobile) bar movement was seen in the sea surface roughness values extracted along the shore parallel transect (Fig. 5). The bars are observed to migrate east by approximately 120 m between the 15/11/2020 and 28/03/2021, and again by ~50 m between 06/09/2021 and 15/02/2022. In contrast, over the interluding summer period (28/03/2021 to 06/09/2021), there is minimal apparent mobilisation.

3.4. Hydrodynamic analysis

The summer and winter migration rates are presented alongside wave power in Table 3. The table shows a clear seasonal distinction both in the distance migrated by the bars (daily rate), but also through the wave power (daily average). Despite this distinction, there was a lower rate of transport during the second winter period, despite nearly

Table 3
Migration rate *vs* daily averaged wave power. N.B. 18 day gap in wave record between 08/01/2021 and 26/01/2021.

Time period	Dates	Duration (days)	Migration distance (m)	Averaged daily migration rate (m day^{-1})	Daily averaged wave power (kW m^{-1})
Winter 20/21	15/11/ 2020 to 28/03/ 2021	132	122.33	0.93	154.38
Summer 21	28/03/ 2021 to 06/09/ 2021	161	9.27	0.06	64.59
Winter 21/22	06/09/ 2021 to 15/02/ 2022	162	50.67	0.31	154.82

identical values for daily-averaged wave power. This could be due to an underestimation of wave power during the Winter 2020/2021 as the wave buoy was out of action for 18 days between the 08/01/2021 and the 26/01/2021.

The seasonal mobilisation trend is presented in a slightly different format in Fig. 6, A. Whilst the trend is clear within Fig. 6 A, the absolute migration rate shows the inherent high variance (Fig. 6, B) within the data, and per transverse finger bar (Fig. 6, C and D). On the whole,

movement of the bars is greater in the winter periods in comparison to the summer, and the net migration is towards the east. During the summer, movement to the west counters movement to the east, and the net change becomes small.

Daily averages and peaks of wave power are shown to be elevated over the winter period in comparison to the summer period, although a large storm event can be observed at the end of May (Fig. 6, E). The wave approach angle shows that waves are typically from the South West, and less frequently arrive from the East. Two periods of sustained easterly waves are observed during the summer, which has a higher incidence of easterly waves than the winter periods (Fig. 6, F).

The frequency distribution of wave parameters, significant wave height, peak wave period and wave direction were shown to vary between the three time periods considered (Fig. 7). The modal wave height was 0.5 m for all periods, however wave heights exceeding 1 m were much more frequent in the winter (Fig. 7, top left). The modal peak period for the winter periods was greater than the summer period (7 s and 3 s respectively) and swell waves were indicated by the presence of secondary peaks around 10 s, suggesting more energetic conditions during the winter periods (Fig. 7, top right). The joint probability showed that the largest wave heights had periods of 5–10 s, whilst the higher energy peak period were associated with small wave heights (>1.0 m), and rarely occurred during the summer, whilst wave heights of up to 3 m had been observed in the summer (Fig. 7, bottom left). Easterly waves were more common in Summer 2020 than the winter periods, and the first winter period (2020/2021) experienced proportionately more easterlies than Winter 2021/2022 (Fig. 7, bottom right).

The weekly mean littoral drift potential and the median bar
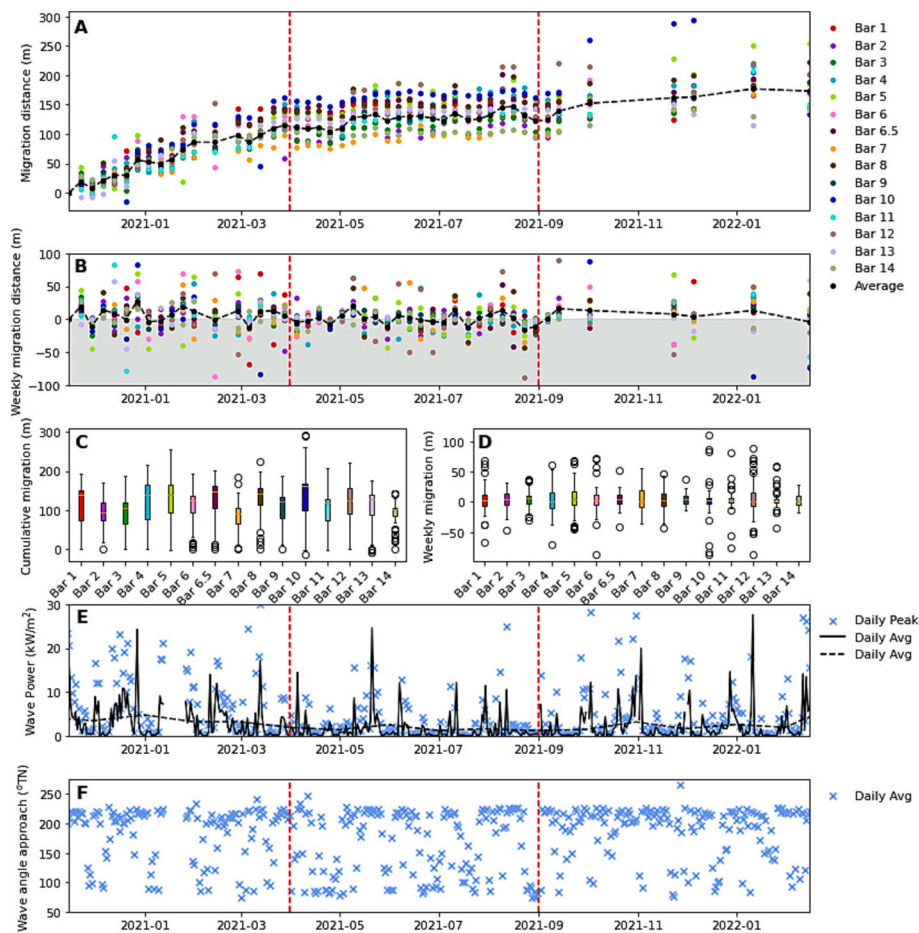
Fig. 6. The migration distances are shown within the observation period both cumulatively (A) and weekly (B) with average values shown by the black marker; followed by cumulative and weekly distance plots for each individual bar, (C) & (D) respectively. The bottom two plots show the wave power (E) and daily average wave direction (F) as recorded by the Pevensey wave buoy.
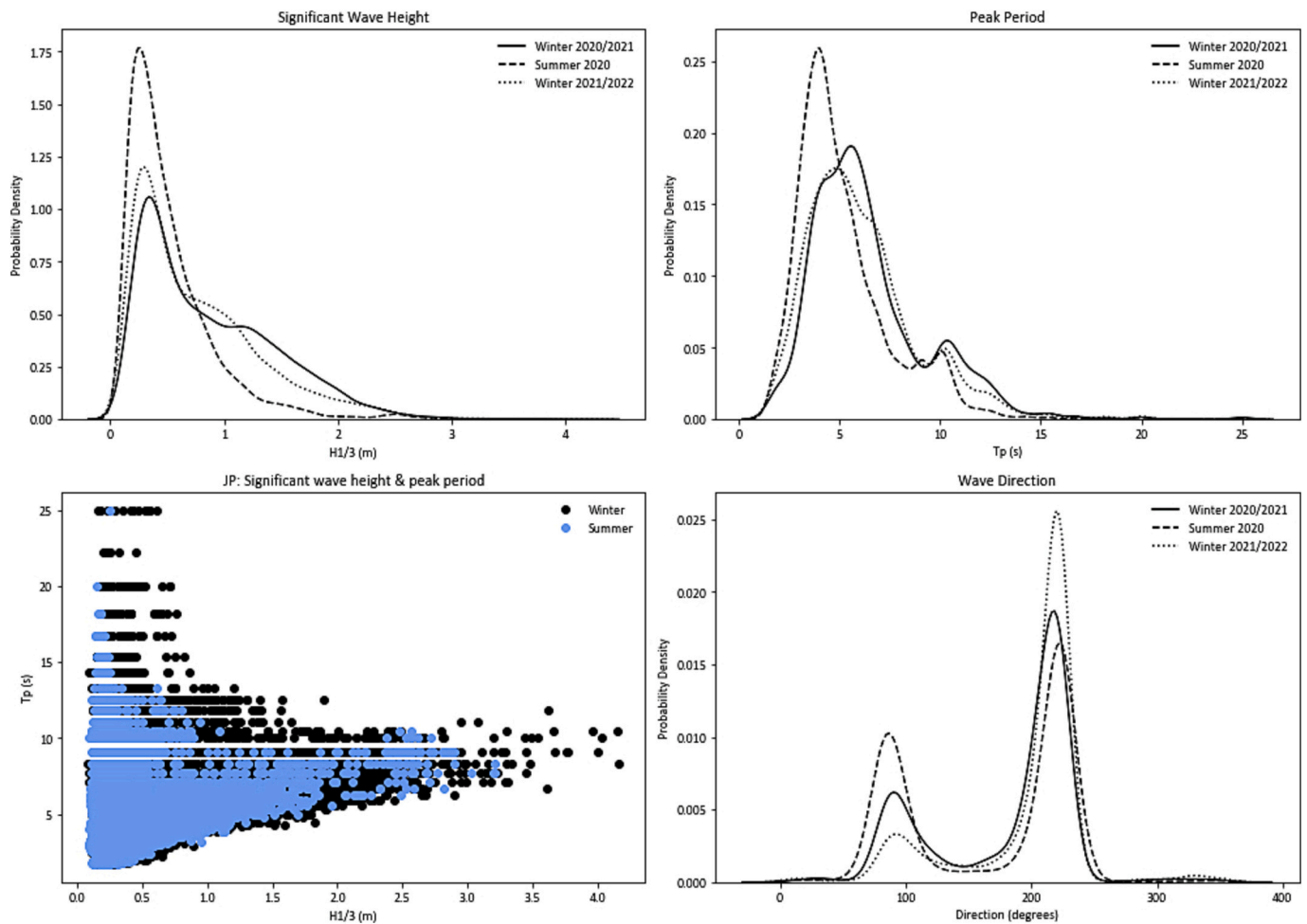
Fig. 7. Distribution of wave height (Hs, top left), peak period (Tp, top right), wave scatter plot (bottom left) and wave direction (bottom right), over the three study periods Winter 2020/2021, Summer 2021, and Winter 2021/2022.

migration was found to have a low positive linear relationship (R^2 value of 0.38), with migration rate increasing with littoral drift potential (Fig. 8). The relationship was found to be statistically significant with $P < 0.001$.

3.5. Upper beach volumetric analysis

Rhythmic, largescale, low-level elevation bedforms can be inferred from the binned difference models of the upper beach from the easterly migration of areas of erosion and accretion over the 19-year observation period (Fig. 9). Notably these bedforms are longshore features and propagate along (from west to east) of the intertidal zone. Although there is a large degree of spatial variation, wavelengths of each feature are approximately 750 m long. The amplitude of the features can be up to ±1.0 m. However, this is minimal considering the long wavelength and prominence of cross-shore structures mixed sand-gravel barrier beach and the ridge runnel system which occasionally develops within the intertidal sandy terrace which fronts the barrier. The bars are migrating by approximately one wavelength every five years, which is equivalent to approximately 150 m per year (measured between ~110 to ~170 m). The winter of 2013/2014 was an especially stormy for the southern coast of England (Dhoop and Mason, 2018) which may be responsible for a large volume of loss at around 2500 m longshore over that time period (Fig. 9).

4. Discussion

There are both similarities and dissimilarities between the morphology, hydrodynamic setting and behaviour of the transverse finger bars identified at Pevensey and other sites recorded in the literature (Table 4). Using Pellón et al.'s (2014) existing classification a new sub-type, 'intermediate energy finger bars', would be required to describe the transverse finger bars found at Pevensey, which could also be used to describe those on the Waddenzee coast as reported by Brakenhoff et al. (2019) (Table 4). Reviewing the existing classifications, we consider there to be only two types of transverse finger bar, those which are 'transient' or 'persistent' following the introduction of the terms by Levoy et al. (2013). This classification ignores the scale of the features (wavelength, crest length and amplitude) as this depends on the sediment type and availability, bed slope and flow velocity of the (combined) wind/tidal/longshore current. The transverse finger bars at Pevensey are persistent, as the 2013 MBES bathymetry and radar imagery extending between November 2020 and February 2022 suggest that the bars have been present within the region for at least ten years. The chevron morphology has not been previously reported and further investigation into the composition and mobility of these lower extensions to the transverse finger bars should be pursued. The change in orientation might suggest refraction of the current, with a reversed near bed flow (Ribas et al., 2003), or alternatively, in the same way that each bar migrates at a different rate, the migration rate also varies across each bar, e.g. the lower part of the bars migrate much slower than the upper part of the bars, and that the chevrons are the beginnings of 'relict'
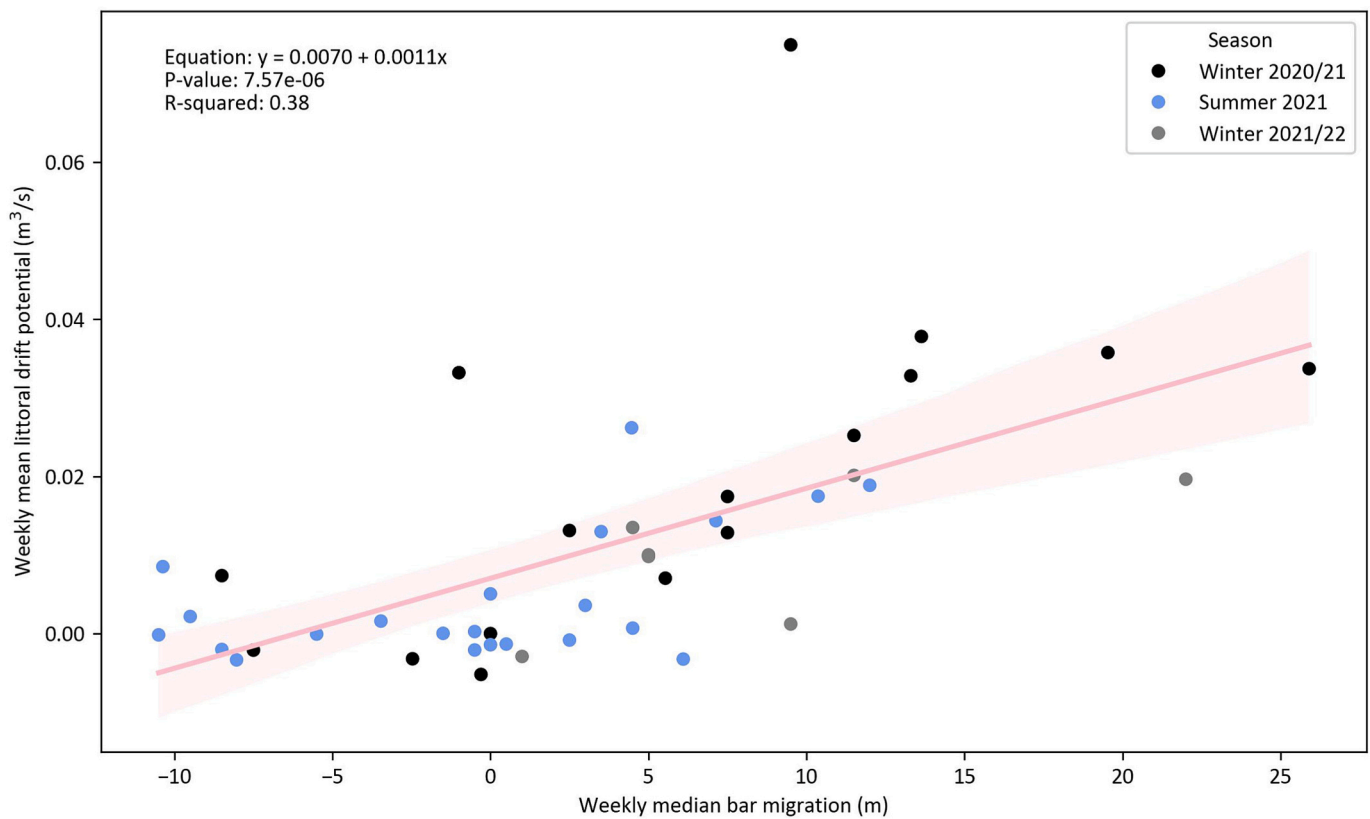
Fig. 8. Linear regression of the weekly mean littoral drift potential (m^3/s) and the weekly median bar migration (m).

features.

The movement of the transverse finger bars was shown to be highly seasonal, with greater movement in the winter/stormy season. The weekly migration rate of the transverse finger bars was found to correlate with the littoral drift potential, with an R^2 of 0.38. Large south westerly waves were highlighted as a key driving condition for net alongshore migration, however, both the bars' migration and the sea surface roughness data are dependent on multivariate conditions. Fast flowing tidal currents at the site may contribute to sediment stirring, encouraging entrainment, and the dominant flood tide may also contribute to the net bar movement. Previous work showed that the site is tidally dominant with tidal currents much larger than the longshore generated current although this is not always the case during storm events (Fugro Emu, 2016). Yet, lack of mobilisation during the summer suggests that tidal currents alone are not strong enough to mobilise the transverse finger bars, but may play an important role in achieving critical flow velocities when the longshore and tidal current are aligned. Moreover, the effects of barometric pressure, negative or positive surges would affect the water depth and therefore the ability of waves to mobilise sediment.

The wider geomorphological and sedimentary setting is unique to the transverse finger bars reported within this study. The grab samples indicated that the surface sediments were comprised of very fine sand at the landward limit of the subtidal features, and the 2013 backscatter image interpretation supports this. However, this sandy area is located within a gravel rich environment, both onshore and offshore (Dornbusch et al., 2005; Mellett et al., 2012). This is visible in the area in which they terminate, as gravel outcrops emerge as part of a complex mosaic in and around the 12th to 14th bar (Fig. 4). It is unknown how mobile the gravel beds are or how much they interact with the mobile features, yet it is likely that they are a permanent feature considering their location at the junction of a decreasing longshore transport gradient, as the coastline changes orientation, and being partially constrained by rock

outcrops to the east (not shown). Shore-oblique bars were strongly correlated with the occurrence of gravel outcrops along the coasts of Virginia and South Carolina, and it was suggested that their presence played a key role in the formation of the features (Schupp et al., 2006). In contrast, at Pevensey, the rhythmic features are not seen beyond (to the east) of the gravel outcrops area, suggesting that the outcrops may play a role in the breakdown of the bedform features.

The rhythmic signatures identified in the upper gravel-rich intertidal beach, have a greater wavelength (750 m) and much wider extent (>9 km) than the transverse finger bars and are therefore likely to be separate features. The migration rates are of the same order of magnitude as the transverse finger bars which hints at a shared driver, but their formation mechanisms are not fully understood. High-angle wave incidence has previously been identified as a driver for shoreline instability (Ashton and Murray, 2006), which have been shown to trigger the formation/migration of intertidal sand waves at sites in Dungeness and El Trubador, Spain, which are also both transverse finger bar sites (Arriaga et al., 2017; Mujal-Colilles et al., 2019). In their comprehensive study of multiple ebb-tidal delta transverse finger bar sites across the Frisian Wadden Islands, Brakenhoff et al. (2019) also highlighted high angle wave instability as the likely driver behind the formation, noting the coincidence of the transverse finger bars and the 'shadow' zone of the larger deltas. Both the transverse finger bar features at Pevensey and Dungeness (Fig. 1) fall within the 'shadow' zone of the predominantly south-westerly incoming waves due to the cuspate forelands and headland located to the west. Whilst high angle wave instability provides a potential explanation for the bar formation, other theories should also be examined further. As bar formation is not directly observed in this study numerical modelling may be used to try and understand the formation of bars at sites such as Pevensey, Dungeness and similar sites, such as the Frisian Wadden Islands (Brakenhoff et al., 2019). To further explore this avenue, field investigations such as direct measurement of waves and currents in the mobile bar area could be used to help derive
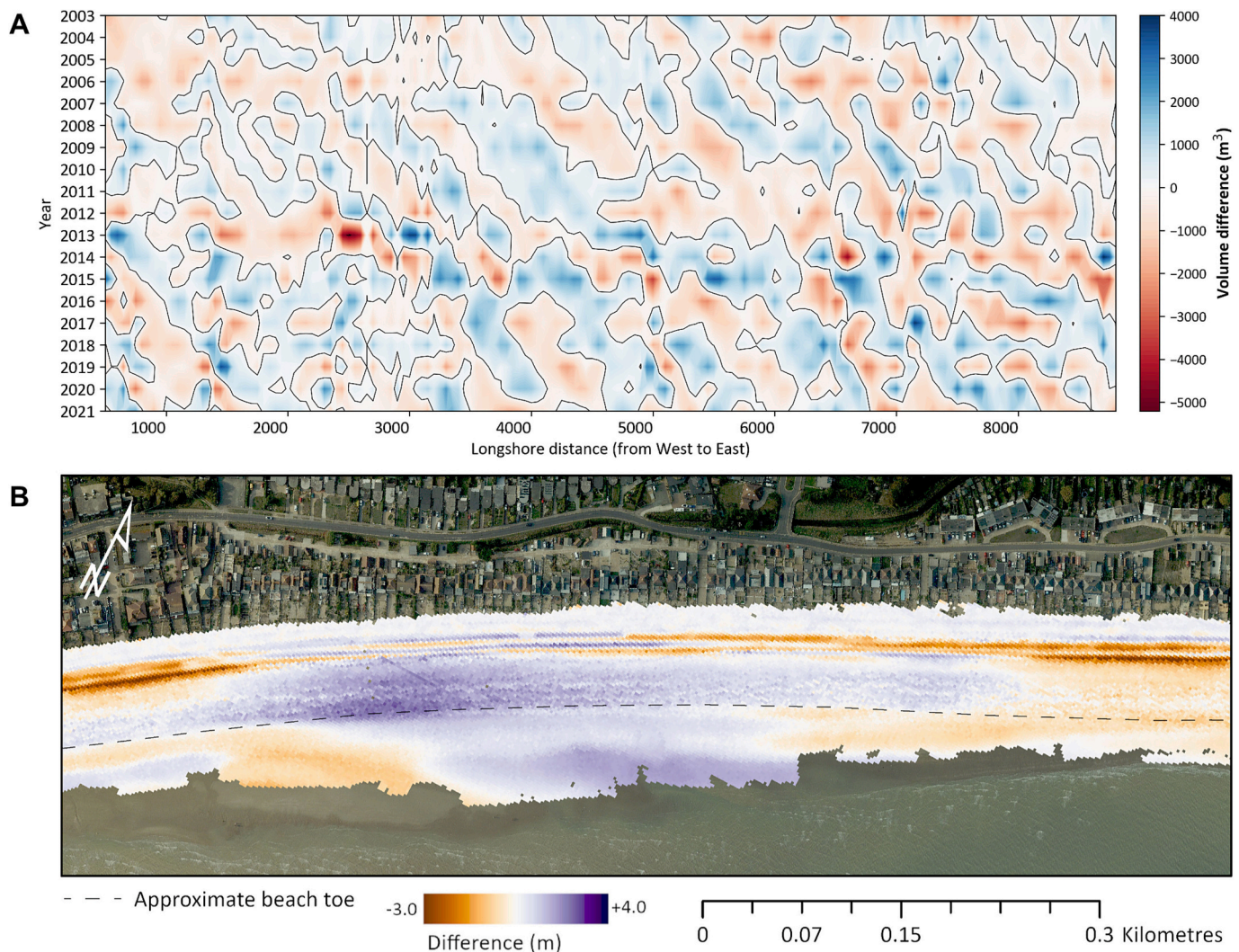
Fig. 9. A) Year on year contour plot for sub-aerial beach surficial change (volumetric) across Pevensey Bay 2003–2022; B) Difference model for the years 2019–2020 at approximately 4400 to 5400 m longshore distance - note the large elevation changes in the upper beach correspond to the berm crest.

the relative importance of different drivers linking to the migration rate and identify key formation mechanisms at the site. Furthermore, data collection which focused on capturing the sub-aerial and sub-tidal down to the depth of closure would enable a better understanding of the rhythmic morphology at this site and any links between features. As hotspots of erosion and accretion align with the crests and troughs of the rhythmic bedforms in the upper intertidal beach, understanding the link between these features and those in the shallow subtidal would be a highly impactful finding for beach managers, working with beach sediments to maintain flood protection, as they do at Pevensey.

5. Conclusions

This study documents the characteristics, movement, and sedimentology of a series of transverse finger bars located within a unique mixed sand-gravel environment, unlike those settings previously reported. Several comparisons to the existing literature are made, and an existing classification is grouped using the wider coastal setting, allowing for a further subtype to accommodate the bars observed at Pevensey which do not currently easily fit into the existing classification. The bars at Pevensey had wavelengths 75 to 375 m, crest lengths between 100 and 700 m, amplitudes were estimated at ~0.2 to ~0.6 m, they were orientated approximately 30° relative to shore normal and were down-current orientated. Grab samples taken from the landward limit of the

bars showed that the surficial sediments comprised fine sand, but gravel outcrops occur within the area of the bars, which are situated in a wider mixed sediment environment. X-band radar was used to create a proxy of the bar's location, showing migration rates ranging between 0.06 and 0.93 m per day, which was significantly related to the potential long-shore transport (0.38 R^2; $P < 0.001$). The bars at Pevensey were shown to display highly seasonal behaviour, migrating in the winter 'stormy' periods when wave heights were highest and largely immobile during the summer months, when wave conditions were largely calm.

CRediT authorship contribution statement

Dominique Townsend: Writing – original draft, Visualization, Methodology, Investigation, Formal analysis, Conceptualization. **Julian Leyland:** Writing – review & editing, Methodology, Conceptualization. **Hachem Kassem:** Writing – review & editing, Methodology, Conceptualization. **Charlie E.L. Thompson:** Writing – review & editing, Methodology, Conceptualization. **Ian H. Townend:** Writing – review & editing, Methodology, Conceptualization. **Paul S. Bell:** Writing – review & editing. **Cai O. Bird:** Writing – review & editing.

Declaration of competing interest

The authors declare the following financial interests/personal

Table 4

The Transverse Finger Bar classification according to persistent and transient types in the context of the wider coastal setting, alongside existing classification from Pellón et al. (2014); and Levoy et al. (2013)). This study shown in bold. N.B. Transverse Bars and Rips are excluded from this table.

Transverse finger bar classification	Type as per Pellón et al. (2014)	Beach description	Beach	Mean wave height (m)	Tidal range (m)	Bar wave-length (m)	Cross-shore span (m)	Bar orientation	Average (min, max) migration rate (m day^{-1})	Observation reference
Persistent	Small-scale low-energy finger bars	Very fetch limited (<10 km)	El Trubador, Spain	0.25	~0.25	15–25; 75 (40–160)	Unknown	Up-current orientated	–	(Falqués, 1989; Mujal-Colilles et al., 2019)
			El Puntal, Bay of Santander, Spain	0.20	5.0	26	70–130	Oblique down-current	0.06 (–, 0.15)	(Pellón et al., 2014)
			Assateague Island, Maryland/ Virginia, USA	<0.1	0.90	13–15	45–75		–	(Bruner and Smosna, 1989)
	Intermediate energy finger bars	**Open coast beaches**	Frisian Wadden Islands, Germany/ Netherlands	1.3;	1.4–3.0	670 (310–900)	800–2200		0.08 (0.005, 0.3);	(Brakenhoff et al., 2019)
			Pevensey Bay, United Kingdom	**>0.5**	**6.7**	**150**	**100–700**		**0.4 (0.06, 0.93)**	*This study*
	Large scale finger bars	Low-energy beaches, wide (~1 km) with gentle slope (0.002)	Contentin coast, Normandy, France	0.46	8.3	110–500	320–1300	Normal or slightly oblique	0.03 (–, 1.0)	(Levoy et al., 2013)
			Anna Maria Island, Florida, USA	0.25	0.7	75–120	~4000		0.02 (0.06)	(Gelfenbaum and Brooks, 2003)
			Popponesset, Cape Cod, Massachusetts, USA	0.24	0.7*	10s–100s	10s–100s		0.03 (0.08)	(Goud and Aubrey, 1985; * Aubrey and Gains, 1982)
			St. James Island, Franklin County, Florida, USA	0.06	–	64–218	107–640		0.05; 0.03–0.06; 0.06 (0.5, 1).	(Niedoroda and Tanner, 1970)
Transient	Intermediate energy finger bars	Intermediate wave-dominated beaches	Surfers Paradise, Gold Coast, Australia	0.81	–	32	–	Up-current orientated	None.	(Ribas et al., 2014)
			Noordwijk, Netherlands	0.67	1.8	21–75	15–60		– (–, 22)	(Ribas and Kroon, 2007)
			Manmade lake, Russia	1.4	0.0	20–30	–		–	(Khabidov, 2001)
			Duck, North Carolina, USA	0.9	0.97	79–172	10–200		– (–, 40)	(Konicki and Holman, 2000)

Appendix A. Supplementary data

Supplementary data to this article can be found online at https://doi.org/10.1016/j.geomorph.2024.109517.

Data availability

Data will be made available on request.

References

Alpers, W., Hennings, I., 1984. Theory of the imaging mechanism of underwater bottom topography by real and synthetic aperture radar. J. Geophys. Res. 89, 10529–10546. https://doi.org/10.1029/JC089iC06p10529.

Amos, C.L., King, E.L., 1984. Bedforms of the Canadian eastern seaboard: a comparison with global occurrences. Mar. Geol. 57, 167–208. https://doi.org/10.1016/0025-3227(84)90199-3.

Arriaga, J., Falques, A., Ribas, F., Crews, E., 2017. Formation and destruction of shoreline sand waves: observations and modelling. Coastal Dynamics 2017, 9–15.

Ashton, A.D., Murray, A.B., 2006. High-angle wave instability and emergent shoreline shapes: 2. Wave climate analysis and comparisons to nature. J. Geophys. Res. Atmos. https://doi.org/10.1029/2005JF000423.

Aubrey, D.G., Gains, A.G., 1982. Recent Evolution of an Active Barrier Beach Complex: Popponesset Beach, Cape Cod, Massachusetts (WHOI-82-3).

Bell, P.S., McCann, D.L., Lawrence, J., Norris, J.V., 2015. Remote detection of sea surface roughness signatures related to subsurface bathymetry, structures and tidal stream turbine wakes. In: Proceedings of the 11th European Wave and Tidal Energy Conference (Nantes).

Bird, C.O., Sinclair, A.J., Bell, P.S., Phillips, M., Green, C., 2019. Autonomous monitoring of nearshore geomorphology and hydrodynamics to assist decision making in coastal management, using shore-based radar systems: A case study on the Fylde peninsula. In: Coastal Management 2019. Institute of Civil Engineers, UK, pp. 201–211. https://doi.org/10.1680/cm.65147.201.

Blott, S.J., Pye, K., 2001. Gradistat: a grain size distribution and statistics package for the analysis of unconsolidated sediments. Earth Surf. Process. Landforms 26, 1237–1248. https://doi.org/10.1002/esp.261.

Boczar-Karakiewicz, B., Bona, J.L., 1986. Wave-dominated shelves: a model of sand-ridge formation by progressive, infragravity waves. In: Knight, R.J., McLean, J.R. (Eds.), Shelf Sands and Sandstones, pp. 163–179. Can. Soc. Petr. Geol., Memoir II.

Brakenhoff, L., Ruessink, G., van der Vegt, M., 2019. Characteristics of saw-tooth bars on the ebb-tidal deltas of the Wadden Islands. Ocean Dyn. 69, 1273–1285. https://doi.org/10.1007/s10236-019-01315-w.

Bruner, K.R., Smosna, R.A., 1989. The movement and stabilization of beach sand on transverse bars, Assateague Island, Virginia. J. Coast. Res. 5, 593–601.

Carter, R.W.G., 1978. Small-scale transverse bars in Lough Neagh, Northern Ireland. Jounal Earth Sci. 1, 205–209.

Channel Coastal Observatory, 2014. Seabed Mapping. Dungeness to Selsey.

Chen, Q., Madsen, P.A., Basco, D.R., 1999. Current effects on nonlinear interactions of shallow-water waves. J. Waterw. Port, Coastal, Ocean Eng. 125, 176–186.

Coco, G., Murray, A.B., 2007. Patterns in the sand: from forcing templates to self-organization. Geomorphology 91, 271–290. https://doi.org/10.1016/j.geomorph.2007.04.023.

Dhoop, T., Mason, T., 2018. Method for Extremes Analysis of Coastal Wave Data, TN01.

Dornbusch, U., Williams, R., Moses, C., 2005. Beach Materials Properties; BAR Phase 1. Science Report.

Elsner, P., Horn, D., DornbuschH, U., Thomas, I., Amos, D., 2015. Monitoring Mixed Sand and Gravel Beaches Using Unmanned Aerial Systems. https://doi.org/10.1142/9789814689977_0172.

Environment Agency, 2017. Regional Beach Management Plan Eastbourne to Rye.

Falqués, A., 1989. Formación de topografía rítmica en el delta del ebro. Rev. Geofísica 45, 143–156.

Falqués, A., Dodd, N., Garnier, R., Ribas, F., MacHardy, L.C., Larroudé, P., Calvete, D., Sancho, F., 2008. Rhythmic surf zone bars and morphodynamic self-organization. Coast. Eng. 55, 622–641. https://doi.org/10.1016/j.coastaleng.2007.11.012.

Falqués, A., Ribas, F., Mujal-Colilles, A., Puig-Polo, C., 2021. A new morphodynamic instability associated with cross-shore transport in the nearshore. Geophys. Res. Lett. 48, 1–9. https://doi.org/10.1029/2020GL091722.

Fugro Emu, 2016. Pevensey Bay, South-east England - Hydrodynamic Study ADP Investigation Report.

Gelfenbaum, G., Brooks, G.R., 2003. The morphology and migration of transverse bars off the west-central Florida coast. Mar. Geol. 200, 273–289. https://doi.org/10.1016/S0025-3227(03)00187-7.

Goud, M.R., Aubrey, D.G., 1985. Theoretical and observational estimates of nearshore bedload transport rates. Mar. Geol. 64, 91–111.

Guza, R.T., Inman, D.L., 1975. Beach Cusps and Edge Waves. Jounral Geophys. Res. 80, 2997–3012. https://doi.org/10.9753/icce.v16.81.

Halcrow, 2010. South Foreland to Beachy Head Shoreline Management Plan. Appendix C: Baseline Process Understanding.

Hartmann, S.S., 2017. Wetland Reclamation in England: Medieval Risk Culture and the 1396 Commission of Sewers for Pevensey Levels. University of Waterloo.

Holman, R., 1995. Nearshore processes. Rev. Geophys. 33, 1237–1247. https://doi.org/10.1029/95RG00297.

Horn, D.P., Walton, S.M., 2007. Spatial and temporal variations of sediment size on a mixed sand and gravel beach. Sediment. Geol. 202, 509–528. https://doi.org/10.1016/j.sedgeo.2007.03.023.

Jennings, S., Smyth, C., 1990. Holocene evolution of the gravel coastline of East Sussex. Proc. Geol. Assoc. 101, 213–224. https://doi.org/10.1016/S0016-7878(08)80006-5.

Khabidov, A., 2001. Transverse bars formation on a tideless beach. In: Coastal Dynamics, pp. 666–672. https://doi.org/10.1061/40566(260)68. Lund, Sweden.

Konicki, K.M., Holman, R.A., 2000. The statistics and kinematics of transverse sand bars on an open coast. Mar. Geol. 169, 69–101. https://doi.org/10.1016/S0025-3227(00)00057-8.

Krumbein, W.C., Pettijohn, F.J., 1938. Manual of Sedimentary Petrography. Appleton-Century-Crofts, New York.

Levoy, F., Anthony, E.J., Monfort, O., Robin, N., Bretel, P., 2013. Formation and migration of transverse bars along a tidal sandy coast deduced from multi-temporal Lidar datasets, 342, 39–52.

Mellett, C.L., Hodgson, D.M., Lang, A., Mauz, B., Selby, I., Plater, A.J., 2012. Preservation of a drowned gravel barrier complex: a landscape evolution study from the north-eastern English Channel. Mar. Geol. 315–318, 115–131. https://doi.org/10.1016/j.margeo.2012.04.008.

Mujal-Colilles, A., Grifoll, M., Falqués, A., 2019. Rhythmic morphology in a microtidal low-energy beach. Geomorphology 334, 151–164. https://doi.org/10.1016/j.geomorph.2019.02.037.

National Network of Regional Coastal Monitoring Programmes., n.d. Pevensey Bay Wave Buoy Statistics: Average Values for All Years [WWW Document]. URL https://coastalmonitoring.org/realtimedata/?chart=77&tab=stats&disp_option=&data_type=table&year=Allyears (accessed 12.11.23).

Nicholls, R.J., 1991. Holocene evolution of the gravel coastline of East Sussex: discussion. Proc. Geol. Assoc. 102, 301–306. https://doi.org/10.1016/S0016-7878(08)80089-2.

Niedoroda, A.W., Tanner, W.F., 1970. Preliminary study of transverse bars. Mar. Geol. 9.

Nieto-Borge, J.C., Jarabo-Amores, P., De La Mata-Moya, D., López-Ferreras, F., 2006. Estimation of ocean wave heights from temporal sequences of X-band marine radar images. Eur. Signal Process. Conf. 1–5.

Pellón, E., Garnier, R., Medina, R., 2014. Intertidal finger bars at El Puntal, Bay of Santander, Spain: observation and forcing analysis. Earth Surf. Dyn. 2, 349–361. https://doi.org/10.5194/esurf-2-349-2014.

Plater, A.J., Stupples, P., Roberts, H.M., 2009. Evidence of episodic coastal change during the late Holocene: the Dungeness barrier complex, SE England. Geomorphology 104, 47–58. https://doi.org/10.1016/j.geomorph.2008.05.014.

Ribas, F., Falque, A., Montoto, A., 2003. Nearshore oblique sand bars. J. Geophys. Res. 108, 1–17. https://doi.org/10.1029/2001JC000985.

Ribas, F., de Swart, H.E., Calvete, D., Falqués, A., 2011. Modelling the formation of transverse sand bars: application to Duck beach, USA. In: Proc. 7th IAHR Symp. River, Coast. Estuar. Morphodynamics.

Ribas, F., Doeschate, A. Ten, De Swart, H.E., Ruessink, B.G., Calvete, D., 2014. Observations and modeling of surf zone transverse finger bars at the Gold Coast, Australia. Ocean Dyn. 64, 1193–1207. https://doi.org/10.1007/s10236-014-0719-4.

Ribas, F., Falqués, A., Deèswart, H.E., Dodd, N., Garnier, R., Calvete, D., 2015. Understanding coastal morphodynamic patterns from depth-averaged sediment concentration. Rev. Geophys. 53, 362–410. https://doi.org/10.1002/2014RG000457.

Ribas, F., Kroon, A., 2007. Characteristics and dynamics of surfzone transverse finger bars. J.Geophys. Res. Earth Surf. 112, 1–13. https://doi.org/10.1029/2006JF000685.

Schupp, C.A., McNinch, J.E., List, J.H., 2006. Nearshore shore-oblique bars, gravel outcrops, and their correlation to shoreline change. Mar. Geol. 233, 63–79. https://doi.org/10.1016/j.margeo.2006.08.007.

Shepard, F.P., 1952. Revised nomenclature for depositional coastal features. Bull. Am. Assoc. Pet. Geol. 36, 1902–1912.

Sonu, C.J., 1968. Collective movement of sediment in littoral environment. Coast. Eng. 1, 373–400. https://doi.org/10.9753/icce.v11.24.

Soulsby, R., 1997. Dynamics of Marine Sands. Thomas Telford, London.

Sutherland, J., Thomas, I., 2011. The management of Pevensey shingle barrier. Ocean Coast. Manag. 54, 919–929. https://doi.org/10.1016/j.ocecoaman.2011.07.004.

Swift, D.J.P., Parker, G., Lanfredi, N.W., Perillo, G., Figge, K., 1978. Shoreface-connected sand ridges on American and European shelves: a comparison. Estuar. Coast. Mar. Sci. 7, 257–273. https://doi.org/10.1016/0302-3524(78)90109-3.

Touboul, J., Morales-Marquez, V., Belibassakis, K., 2024. A weakly nonlinear system for waves and sheared currents over variable bathymetry. J. Mar. Sci. Eng. 12. https://doi.org/10.3390/jmse12030509.

Townsend, D., Leyland, J., Kassem, H., Thompson, C., Townend, I., 2024. Exploring nearshore bed dynamics of a mixed beach using the depth of closure conceptual model. Geomorphology 454, 109150. https://doi.org/10.1016/j.geomorph.2024.109150.

Weggel, J.R., 1972. Maximum Breaker Height. J. Waterw. Harb. Coast. Eng. Div. 98.